ADVANCED MATERIALS

www.advmat.de

Room-Temperature Ferromagnetic Insulating State in Cation-Ordered Double-Perovskite $Sr_2Fe_{1+x}Re_{1-x}O_6$ Films

*Changhee Sohn, Elizabeth Skoropata, Yongseong Choi, Xiang Gao, Ankur Rastogi, Amanda Huon, Michael A. McGuire, Lauren Nuckols, Yanwen Zhang, John W. Freeland, Daniel Haskel, and Ho Nyung Lee**

Ferromagnetic insulators (FMIs) are one of the most important components in developing dissipationless electronic and spintronic devices. However, FMIs are innately rare to find in nature as ferromagnetism generally accompanies metallicity. Here, novel room-temperature FMI films that are epitaxially synthesized by deliberate control of the ratio between two B-site cations in the double perovskite $Sr_2Fe_{1+x}Re_{1-x}O_6$ ($-0.2 \le x \le 0.2$) are reported. In contrast to the known FM metallic phase in stoichiometric Sr_2FeReO_6, an FMI state with a high Curie temperature ($T_c \approx 400$ K) and a large saturation magnetization ($M_S \approx 1.8\ \mu_B$ f.u.$^{-1}$) is found in highly cation-ordered Fe-rich phases. The stabilization of the FMI state is attributed to the formation of extra Fe^{3+}—Fe^{3+} and Fe^{3+}—Re^{6+} bonding states, which originate from the relatively excess Fe ions owing to the deficiency in Re ions. The emerging FMI state created by controlling cations in the oxide double perovskites opens the door to developing novel oxide quantum materials and spintronic devices.

High Curie temperature (T_c) ferromagnetic insulators (FMIs) are critical for realizing dissipationless quantum electronic/spintronic devices and solid-state quantum computing.[1] FMIs are essential to filter electronic charges to generate pure spin currents, to manipulate spins in nonmagnetic layers by magnetic proximity effect,[2–4] and to create a quantum anomalous Hall effect in combination with topological insulators.[5,6] Unfortunately, the ferromagnetism generally accompanies metallicity in nature. The most common mechanism for ferromagnetism is the Ruderman–Kittel–Kasuya–Yosida (RKKY) interaction,[7–9] where itinerant electrons mediate FM interactions among local spins. Such an interaction, therefore, is completely suppressed in insulating materials, and an antiferromagnetic ground state generally emerges. While oxide perovskites are promising materials for future technologies owing to the rich correlated phenomena, such as unconventional superconductivity, colossal magnetoresistance, ferroelectricity, and metal–insulator transition, only few perovskite FMIs are known and their magnetic transitions occur at low temperatures (T).[10]

The 3d–5d double-perovskite system ($A_2B'B''O_6$) is a promising candidate for FMIs because of the unique mechanism of their ferromagnetism and different nature of 3d and 5d orbitals. Double perovskites are compatible with other oxide perovskites owing to the similar crystallographic structure. The two different B-site cations are known to order in the checkerboard type as shown in **Figure 1**a. Since some of these compounds are ferromagnetic metals (FMMs) above room T, they have been considered as a promising candidate for spintronic devices.[11–16] The uniqueness of the ferromagnetism in these materials is that it originates from the so-called hybridization mechanism instead of the RKKY interaction.[17] In the hybridization mechanism, high-T_c ferromagnetism is stabilized by large exchange splitting of one of the two magnetic ions and spin-dependent hybridization between the two B-site d orbitals.[11,18] Since itinerant electrons do not play a role in inducing ferromagnetism, the latter can be robust against the depletion of free carriers. Among those double perovskites, particular attention is paid to systems composed of 3d and 5d transition metal ions, which have potential to show a wide range of electronic and magnetic ground states owing to the cooperative/competitive interactions between strongly localized 3d orbitals and extended/spin-orbit coupled 5d orbitals.

Dr. C. Sohn, Dr. E. Skoropata, Dr. X. Gao, Dr. A. Rastogi, A. Huon, Dr. M. A. McGuire, Dr. Y. Zhang, Dr. H. N. Lee
Materials Science and Technology Division
Oak Ridge National Laboratory
Oak Ridge, TN 37831, USA
E-mail: hnlee@ornl.gov

Dr. Y. Choi, Dr. J. W. Freeland, Dr. D. Haskel
Advanced Photon Source
Argonne National Laboratory
Argonne, IL 60439, USA

A. Huon
Department of Materials Science & Engineering
Drexel University
Philadelphia, PA 19104, USA

L. Nuckols, Dr. Y. Zhang
Department of Materials Science and Engineering
University of Tennessee
Knoxville, TN 37996, USA

DOI: 10.1002/adma.201805389

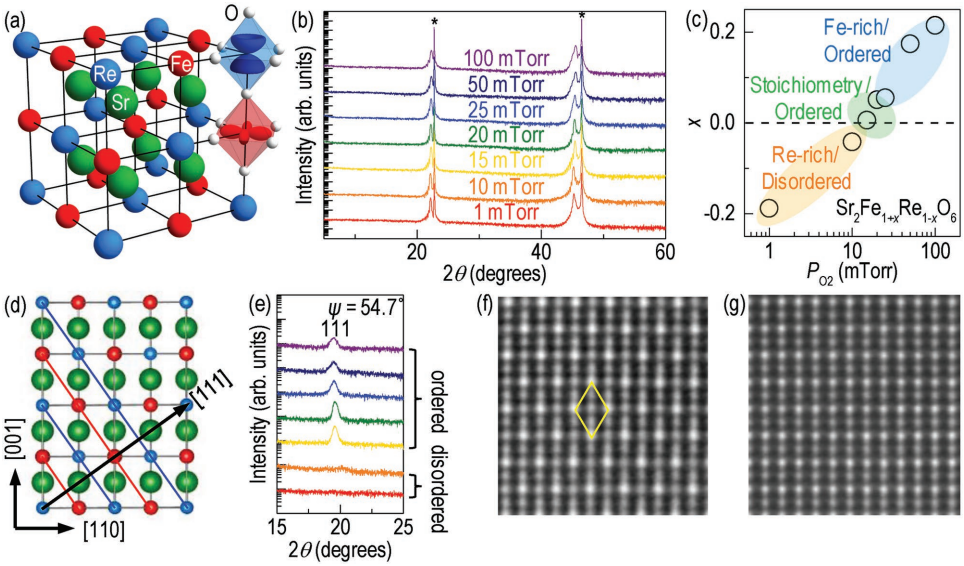

Figure 1. Epitaxial growth of highly cation-ordered $Sr_2Fe_{1+x}Re_{1-x}O_6$ films. a) Schematic of the double perovskite Sr_2FeReO_6. Spin-orbit coupled 5d wave function and localized 3d wave function are visualized inside octahedra. b) XRD θ–2θ scans for $Sr_2Fe_{1+x}Re_{1-x}O_6$ films on $SrTiO_3$ grown at 775 °C under different P_{O_2}. Asterisks indicate peaks from the $SrTiO_3$ substrate. c) x values in $Sr_2Fe_{1+x}Re_{1-x}O_6$ formula obtained from RBS measurements as a function of P_{O_2}. d) A schematic of the projected double-perovskite structure along the [110] direction. The blue and red lines are alternating atomic planes of Re and Fe along the [111] direction, respectively. The [111] direction is indicated with a black arrow. e) Off-axis XRD θ–2θ scans near the $Sr_2Fe_{1+x}Re_{1-x}O_6$ 111 peak. Its appearance confirms the Fe/Re ordering. f,g) HAADF images of a cation-ordered film grown at 20 mTorr (f) and a disordered film grown at 1 mTorr (g). The yellow diamond in (f) highlights the ordered Re ions.

Here, we report a way to synthesize highly insulating double-perovskite epitaxial films with high-T_c ferromagnetism (≈400 K) by properly controlling the ratio and ordering of two cations in $Sr_2Fe_{1+x}Re_{1-x}O_6$ ($-0.2 \le x \le 0.2$) systems. We found that, when other growth parameters are optimized, a single growth parameter, oxygen partial pressure, can be utilized to widely tune the ratio between two B-site cations Fe and Re. In addition to the original FMM state, which can be found when the Fe/Re ratio is balanced, FMI states are obtained in the growth regime of Fe-rich and cation-ordered phases. The room-T sheet resistance of insulating films are about three orders of magnitude larger than that of metallic films. X-ray absorption and optical spectroscopy further revealed that the formation of Fe^{3+}—Fe^{3+} and Fe^{3+}—Re^{6+} bonding is responsible for the insulating electronic structure in Fe-rich films.

We used pulsed laser deposition with a sintered Sr_2FeReO_6 target to synthesize high-quality $Sr_2Fe_{1+x}Re_{1-x}O_6$ epitaxial thin films on (001) $SrTiO_3$ substrates. The latter are thermally and chemically treated to achieve atomically flat, TiO_2-terminated surfaces. For crystallographic parameters, we treated our films as pseudocubic with a slight tetragonal distortion ($a_{pc} = b_{pc} = 7.864$ Å and $c_{pc} = 7.901$ Å for the case of stoichiometric bulk sample) to match the crystallographic direction with that of the cubic substrate.[19] It is known that the growth of double-perovskite thin films is sensitive to many growth parameters, including oxygen pressure (P_{O_2}), substrate T, and growth rate.[20–24] Among many growth parameters, we found that P_{O_2} was the most critical growth parameter affecting the ratio and cation ordering in $Sr_2Fe_{1+x}Re_{1-x}O_6$ films. Figure 1b exhibits X-ray diffraction (XRD) θ–2θ scans of films grown under various P_{O_2} at fixed $T = 775$ °C. Note that, within the whole range of P_{O_2}, high-quality epitaxial films with perovskite structures were obtained.

Rutherford back-scattering spectrometry (RBS) experiments revealed that x, the stoichiometry between two B-site cations (Fe and Re), can be widely controlled only by P_{O_2}. Each RBS spectrum for a film grown with different P_{O_2} was fitted to extract the quantitative portion of Sr, Fe, and Re ions in the film. While the signals from Fe and Re ions were clearly resolved from the substrate signal, Sr signal from the substrate makes it difficult to accurately measure the portion of Sr ions in films. Nevertheless, fitting values for the amount of Sr ions in every film turned out to be comparable to the sum of Fe and Re ions. Figure 1c shows x values from the RBS spectra as a function of the growth P_{O_2}. A clear trend was observed; x increases as the growth P_{O_2} increases. Note that stoichiometric ($x \approx 0$) films were obtained only in the very narrow P_{O_2} range from 10 to 25 mTorr while films grown below 10 mTorr become Re-rich phases ($x < 0$) and films grown above 25 mTorr become Fe-rich phases ($x > 0$). This observation confirms that relative ratio between Fe and Re ions can be precisely controlled only by simple growth parameter, P_{O_2}. Such a large tunable stoichiometry by growth pressure is unusual but not impossible as a previous study on double-perovskite Sr_2MoFeO_6 films demonstrated.[25] In our films, we speculate that a highly volatile ReO_3 phase may attribute to such a large stoichiometry tuning by P_{O_2}. ReO_3 phase is extremely volatile so that it sublimates even at 200 °C.[26] Since this phase is one of the highest oxidized states of Re, ReO_3 will more likely occur during growth with high P_{O_2}. Then, these vacant positions of Re ions could be occupied by Fe ions owing to the nonequilibrium process of pulsed laser deposition and its similar ionic radius (Fe^{3+}: 78.5 pm) with the Re

ions (Re^{5+}: 72 pm), consistent with our observation of Fe-rich phases in high P_{O_2}.

In addition to cation stoichiometry confirmed by RBS, one can expect the oxygen stoichiometry might depend on P_{O_2} as well, which is very difficult to rule out completely in most cases. We conjecture, however, that the amount of oxygen vacancies in our films is insignificant due to the following reasons: First, our films are compressively strained. It is known that the formation of oxygen vacancies is less likely in compressively strained perovskites compared to tensile strained perovskites due to kinetic and thermodynamic limitations.[27–29] We therefore expect that the compressive strain induced by the $SrTiO_3$ substrate helps suppress the formation of oxygen vacancies relative to the case of tensile strain. Second, the lattice parameters of the entire films did not show any reduction when postannealed. Note that oxygen vacancies in most perovskites are known to yield expanded lattice parameters. Therefore, if there were noticeable oxygen vacancies in our samples, we could expect a shift XRD peak positions with postannealing as oxygen vacancies are compensated. However, postannealing experiments with our films did not show any shrinkage of the lattice parameters. Third, the valence of Fe (Re) ions in our stoichiometric films ($x \approx 0$) turned out to be close to 3+ (5+) in X-ray absorption spectroscopy (XAS) spectra, implying the fully oxidized states. We, therefore, conclude that P_{O_2} mainly controls the relative ratio between two cations, while barely affecting the Sr and O stoichiometry, validating our chemical formula $Sr_2Fe_{1+x}Re_{1-x}O_6$.

Another important structural parameter for double perovskites is cation ordering of Fe and Re ions. When B-site cations are ordered in the checkerboard type, they are alternatively stacked along the [111] direction as highlighted by the red and blue lines in Figure 1d. This ordering is confirmed by XRD off-axis scans at $\psi = 54.7^{\circ}$ near the Sr_2FeReO_6 111 peak. As shown in Figure 1e, the 111 peak is only observable for films grown with a P_{O_2} higher than 15 mTorr. Such a cation ordering is further confirmed by scanning transmission electron microscopy (STEM). The schematic drawing in Figure 1d shows a projected structure of Sr_2FeReO_6 along the [1-10] direction. The two B-site cations are ordered along the projected direction, so that they can be resolved by high-angle annular dark field (HAADF) imaging.[30] In HAADF images, Re ions (atomic number $Z = 75$) give the brightest intensity, while the intensity of Sr ($Z = 38$) and Fe ($Z = 26$) ions is less intense as they are lighter than Re. Figure 1f is a HAADF image of a cation-ordered film grown at 20 mTorr. The clear ordering highlighted by the yellow diamond is observed as expected from the Re position of ordered double perovskite shown in Figure 1d. In the HAADF image of the disordered film grown at 1 mTorr (Figure 1g), on the other hand, such ordering was destroyed, which can be confirmed by a uniform contrast for all the B sites. This observation is consistent with the disappearance of the 111-ordering peak in XRD scans for the samples grown in low P_{O_2} (<15 mTorr). From the RBS, XRD, and STEM experiments, we conclude that the P_{O_2} must be well balanced in three regimes, i.e., low P_{O_2} (<15 mTorr), P_{O_2} near 20 mTorr (15–25 mTorr), and high P_{O_2} (>25 mTorr), to make disordered/Re-rich, ordered/stoichiometric, and ordered/Fe-rich phases, respectively, as illustrated in Figure 1c.

It should be noted that cation-ordered films are only obtained in stoichiometric and Fe-rich films ($x \geq 0$) while Re-rich films ($x < 0$) preferred to be disordered. Although cation ordering and ratio might be independently affected by detailed growth mechanisms, the tendency of cation disordered states in Re-rich phases could be understood in terms of an auxiliary effect from the change of stoichiometry. One of the most important factors for cation ordering is how much the ionic radii of two cations are different: if the radii of two B-site cations are similar, the cation ordering would be more difficult. According to our XAS spectra, which will be discussed in detail later, valence of Fe ions remains as 3+ in entire set of samples while valence of Re ions changes from 4+ in Re-rich phases to 6+ in Fe-rich phases to satisfy charge neutrality. Note that, ionic radii of Re^{4+} ions is 77 pm, which is very close to the ionic radii of Fe ions (78.5 pm). On the other hand, Re^{5+} and Re^{6+} ions have ionic radius of 72 and 69 pm, different enough from that of Fe^{3+} to have cation ordering. This explanation is consistent with our observation that there is cation ordering in stoichiometric and Fe-rich phases but not in Re-rich phases.

We investigated the evolutions of magnetic and electronic ground states in our $Sr_2Fe_{1+x}Re_{1-x}O_6$ films. **Figure 2**a–c display magnetization (M) versus T curves, M versus magnetic field (H) curves, and T-dependent sheet resistance $R_S(T)$ of three characteristic samples, Re-rich/disordered ($x \approx -0.2$, P_{O_2} = 1 mTorr), stoichiometric/ordered ($x \approx 0.05$, P_{O_2} = 20 mTorr), and Fe-rich/ordered ($x \approx 0.2$, P_{O_2} = 100 mTorr) films, respectively. The cooling and measuring field for $M(T)$ curves was 1000 Oe, and the $M(H)$ curves were measured at 10 K. We first focused on the stoichiometric/ordered film (indicated by green lines). The $M(T)$ curve was consistent with typical of long-range ferromagnetic ordering. To check the T_c of the films, we further obtained saturated magnetization (M_S) data at high T. The results are shown as open circles in the Figure 2a. From the data, a T_c near 400 K was determined to be similar to previous reports of 390–410 K for bulk samples.[31–33] The $M(H)$ curve in Figure 2b for the ordered/stoichiometric film shows a clear hysteresis behavior as well. The M_S of 2.0 ± 0.1 μ_B f.u.$^{-1}$ lower than the ideal value 3.33 μ_B f.u.$^{-1}$ was likely due to potential antisite disorder in films, a typically problem in all double-perovskite materials.[16] In particular, a thorough study on polycrystalline Sr_2FeReO_6 revealed that the magnetism in Sr_2FeReO_6 is known to be more sensitive to the amount of antisite disorders than other double perovskites.[30] According to their empirical relationship between M_S and amount of antisite disorder, the observed M_S of 2.0 μ_B f.u.$^{-1}$ implies ≈12% of antisite disorders in our films. The electronic ground state for the stoichiometric/ordered film is metal because their $R_S(T)$ in Figure 2c showed a negligible T dependence with decreasing T only with small upturns at low T from the impurity scattering. Therefore, ground state of our stoichiometric/ordered film is described as FMM, consistent with polycrystalline bulk results.[32]

While the original ferromagnetic ground state was observed in the Fe-rich/ordered films but completely disappeared in the Re-rich/disordered film, the metallic ground state was more vulnerable to excess Fe ions than excess Re ions. In Fe-rich/ordered films (blue lines), we observed a clear magnetic transition near 400 K as well as hysteresis behavior with the $M_S \approx 1.8$ μ_B f.u.$^{-1}$ as shown in Figure 2a,b. For Re-rich/disordered films (red lines),

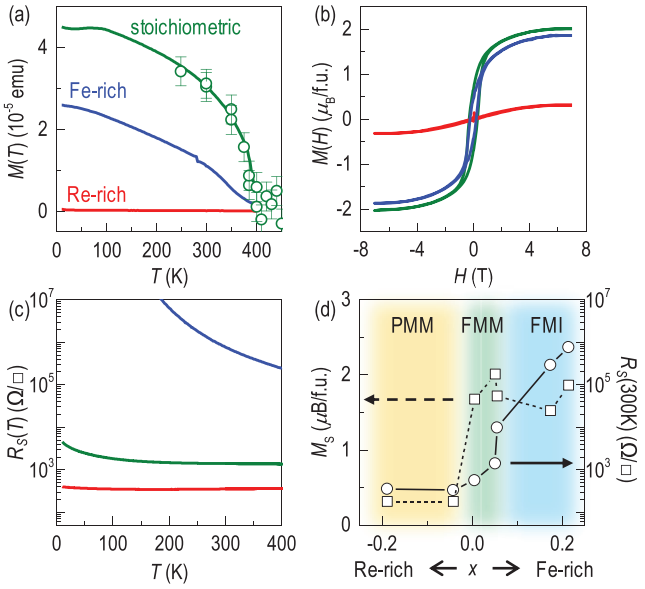

Figure 2. Metal–insulator transition with robust ferromagnetism above room temperature. a) $M(T)$ curves with field cooling and measuring at 1000 Oe. Red, green, and blue lines are $M(T)$ curves of Re-rich, stoichiometric, and Fe-rich films. Green open circles are $M_S(T)$ data obtained by a high-T oven setup for a stoichiometric film to determine the T_c. Due to the instrumental size limitation of the sample holder for the high-T oven setup, isothermal magnetization curves were obtained between 4 and −4 kOe. The data above 1 kOe and below −1 kOe were fit with a line to estimate the M_S of the sample at Ts between 250 and 500 K. An arbitrary constant was multiplied to overlap with an $M(T)$ curve. b) $M(H)$ curves at 10 K. Clear hysteresis behaviors were observed in stoichiometric and Fe-rich films but not in the Re-rich/disordered film. c) Semi-log plot of $R_S(T)$: while Re-rich and stoichiometric films show metallic behaviors, a clear insulating behavior was observed in Fe-rich film. d) R_S(300 K) and M_S as a function of x in $Sr_2Fe_{1+x}Re_{1-x}O_6$. PMM, FMM, and FMI ground states are stabilized in Re-rich/disordered, stoichiometric/ordered, and Fe-rich/ordered phases, respectively.

on the other hand, long-range magnetic ordering is completely destroyed, as evidenced in no T-dependence in $M(T)$ curves and lack of hysteresis in $M(H)$. A small but finite value of magnetization in disordered samples at high fields may imply the presence of the short-range magnetic ordering or spin-glass behaviors. From the above speculation about insignificant amount of oxygen vacancies in our films, we attributed this abrupt disappearance of long-range ordering in Re-rich films to the absence of B-site cation ordering, known to play a critical role in ferromagnetic ground states in double-perovskite systems. In contrast to the magnetism, the metallic ground state was preserved in Re-rich/disordered films as $R_S(T)$ in Figure 2c showed a negative T dependence with decreasing T. However, for the case of Fe-rich films, a clear insulating behavior was observed. It should be noted that variation of room-T resistivity is about three orders of magnitude. The observed metal–insulator transition in our single crystalline films is more dramatic than that reported for polycrystalline $Sr_2Fe_{1+x}Re_{1-x}O_6$,[34] which can be attributed to the absence of metallic grain boundaries in our film that are often found in polycrystalline films. As summarized in Figure 2d, the magnetometry and transport experiments revealed paramagnetic metal (PMM), FMM, and room-temperature FMI in Re-rich/disordered ($x < 0$), stoichiometric/ordered ($x \approx 0$) and Fe-rich/ordered ($x > 0$) $Sr_2Fe_{1+x}Re_{1-x}O_6$ films, respectively.

We used XAS to gain a deeper understanding of the FMI state in Fe-rich films. The top panel of **Figure 3**a shows total electron yield (TEY) XAS spectra near the Fe L_3 and L_2 edges of a Re-rich PMM, stoichiometric FMM, and Fe-rich FMI films. By comparing with the reference Fe^{2+}, Fe^{3+}, and Fe^{4+} spectra in the bottom panel,[35,36] we found that the spectral features from metallic and insulating films were overall similar to those of octahedral Fe^{3+}. The two-peak structure in Fe L_3 and L_2 edges originates from the transitions from 2p core levels to empty 3d t_{2g} and e_g orbitals. The only noticeable change we found in the FMI film is that the peaks for unoccupied t_{2g} orbitals are better resolved and have a higher intensity than those from metallic films. Similar trends have been observed in fluorescence yield (FY) spectra (the inset of Figure 3a), indicating that such a spectral change did not originate from the surfaces. While the formation of Fe^{2+} ions may explain the increased intensity at the t_{2g} peaks, such formation is unlikely in Fe-rich phases, where Fe should prefer to be Fe^{4+} for charge neutrality. The formation of Fe^{4+} ions, known to broaden L-edge XAS spectra significantly, is also inconsistent with our observation that the spectrum of the Fe-rich FMI film shows shaper t_{2g} and e_g peaks than those of the PMM and FMM films. In addition, a previous Mössbauer study on $Sr_2Fe_{1+x}Re_{1-x}O_6$ polycrystalline samples revealed the robust trivalent Fe^{3+} state is maintained in Fe-rich samples.[34] We found that the decrease in the hybridization between the Fe 3d and Re 5d orbitals owing to the Re deficiency can explain this spectral change. In this double perovskite, there is strong hybridization between Fe 3d and Re 5d orbitals, which induces charge transfer from the Re t_{2g} to Fe t_{2g} orbitals.[17] Therefore, Re deficiency would reduce the amount of the charge transfer, resulting in enhancement of the unoccupied density of states (DOS) of Fe t_{2g} orbitals.

In contrast to the robust trivalent Fe valence, the valence of Re ions is modified in $Sr_2Fe_{1+x}Re_{1-x}O_6$ films. Figure 3b shows XAS spectra of PMM, FMM, and FMI films of Re L_3 and L_2 edges (the top panel) together with reference spectra of Re^{4+}, Re^{5+}, and Re^{6+} (the bottom panel).[37] The black dashed line indicates the center position of the Re^{4+} spectrum. As shown in the reference spectra, a characteristic feature of changes in Re valences is that spectral weight of the peak shifts to higher energy as Re valence increases. A similar trend has been observed in our $Sr_2Fe_{1+x}Re_{1-x}O_6$ films as x increased. Compared to stoichiometric films with 5+ Re valence, the center energy of the peak of the Re-rich PMM film shifted to lower energy, indicating the presence of Re^{4+} ions. On the other hand, spectral weight of the peak of the FMI film with excess Fe moved to higher energy, indicating the emergence of Re^{6+} ions. To examine such evolutions in spectra more clearly, we subtracted the spectrum of an FMI film from that of a stoichiometric FMM film ($I_{FMI} - I_{FMM}$). These spectral changes are very similar to the difference between Re^{6+} and Re^{5+} reference spectra ($I_{Re6+} - I_{Re5+}$). It is a natural consequence of the robust trivalent Fe^{3+} ions, which requires a higher oxidation state of Re ions for charge neutrality in the Fe-rich phase. Note that, the substitution of a Re^{5+} ion for an Fe^{3+} ion will introduce two additional Re^{6+} ions to maintain the average valence of B-site cations as 4+ as confirmed from the XAS data.

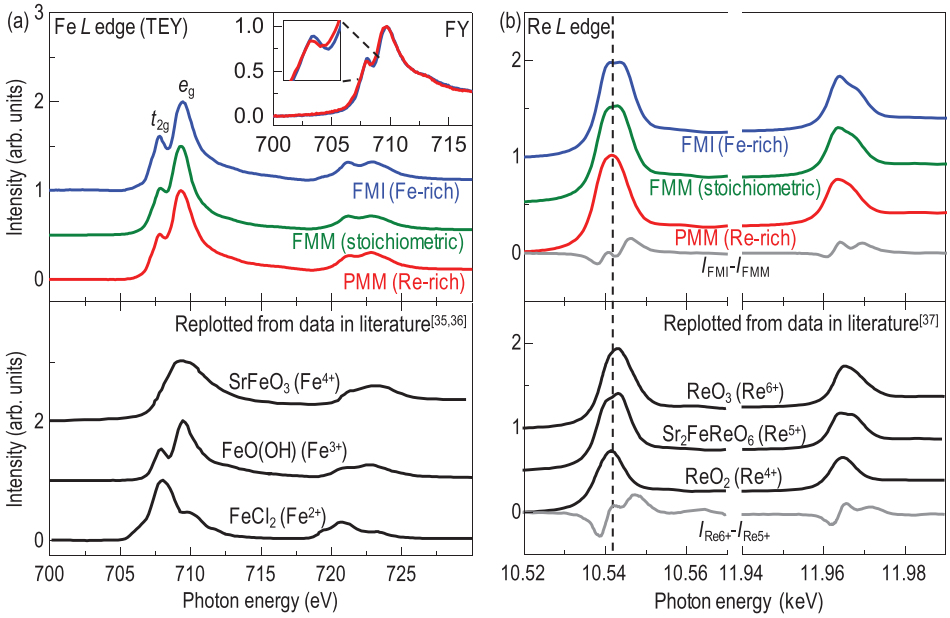

Figure 3. Fe and Re valence changes in XAS spectra. a) Fe *L*- and b) Re *L*-edge XAS spectra of PMM, FMM, and FMI films (top panels); the reference spectra (bottom panels) are replotted from data presented in previous reports.[35–37] Fe *L*-edge spectra show a small change among films except a slight increase of the peak intensity of unoccupied t_{2g} orbitals in the FMI film. This result indicates the reduced hybridization between Re 5d and Fe 3d orbitals. The inset of (a) shows FY spectra near the Fe L_3 edge of PMM and FMI films, validating that the observed spectral change in TEY is not coming from the surfaces. In Re *L*-edge spectra, on the other hand, spectral weight changes indicate the presence of Re^{4+} (Re^{6+}) ions in the Re-rich (Fe-rich) film.

We found that the excess Fe^{3+} ions and emergence of Re^{6+} ions are keys to understand the dramatic increase of resistance of the Fe-rich phase. In this regime, there are three bonding types connecting the nearest B-site cations, i.e., Fe^{3+}—Re^{5+}, Fe^{3+}—Fe^{3+}, and Fe^{3+}—Re^{6+}. As shown in **Figure 4**a, we can draw schematics of local DOS for each bonding based on density functional theory (DFT) calculations of A_2FeReO_6,[38] $LaFeO_3$,[39] and Sr_2FeWO_6.[17] For the original Fe^{3+}—Re^{5+} bonding in stoichiometric samples, Re 5d orbitals are located below Fe 3d orbitals. Strong hybridization and charge transfer between Fe 3d and Re 5d orbitals, therefore, induce dispersive band structures crossing the Fermi level (E_F), yielding the metallic behavior. On the other hand, the Fe^{3+}—Fe^{3+} bonding found in, for example the simple perovskite $LaFeO_3$,[39] is known to result in an insulating state due to the strong Coulomb interaction. The Fe^{3+}—Re^{6+} bonding is expected to show an insulating nature as the Fe^{3+}—Re^{6+} bonding is the same as the Fe^{3+}—W^{5+} bonding in the insulating Sr_2FeWO_6. A previous DFT calculation explained that strong hybridization between extended W $5d^1$ and O 2p orbitals pushes the W 5d orbitals above the Fe 3d orbitals, disturbing the charge transfer and, thereby, stabilizing an insulating ground state.[17] Similar arguments can be applied to the Re^{6+} $5d^1$ orbitals, implying an insulating nature for the Fe^{3+}—Re^{6+} bonding. Since one substitution of one Re^{5+} ion with an Fe^{3+} ion introduces not only one Fe^{3+}—Fe^{3+} but also two Fe^{3+}—Re^{6+} bondings, this modification in turn triples the effectiveness of stabilizing the insulating ground state.

Optical spectroscopy further confirms the schematic DOS shown in Figure 4a. Figure 4b shows the real part of optical conductivity $\sigma_1(\omega)$ between 1.2 and 5 eV of PMM, FMM, and FMI films measured by a spectroscopic ellipsometer. For the original Re^{5+}—Fe^{3+} bonding of stoichiometric Sr_2FeReO_6, one can expect two types of optical transitions: d-d transitions between Re 5d and Fe 3d orbitals (labeled as *A* in Figure 4a) and p-d transitions from O 2p to Re/Fe d orbitals (*B* in Figure 4a). As expected, we observed two distinct spectral features, i.e., a broad spectral weight below 2.5 eV (*A*) and a strong peak near 4 eV (*B*), in $\sigma_1(\omega)$ of a FMM film (green line), consistent with previous bulk data.[40] In the FMI film, on the other hand, spectral weights of *A* and *B* were dramatically reduced while a new peak denoted as *C* emerged. The peak *C* could be assigned as transitions from O 2p to Fe 3d orbitals in the Fe^{3+}—Fe^{3+} bonding in Figure 4a, similar to a previous optical study on $La^{3+}Fe^{3+}O_3$.[41] We did not observe any absorption expected from the Fe^{3+}—Re^{6+} bonding, i.e., transitions from O 2p to Re/Fe d orbitals, in this accessible energy regime. As shown in the schematic diagram in Figure 4a, O 2p states of this bonding state is farther from E_F than those of other two bonding states by the strong O 2p–Re $5d^1$ hybridization, which yields the corresponding optical transitions at higher energies than our instrumental limit.

It is worthwhile to compare FMI states observed in $Sr_2Fe_{1+x}Re_{1-x}O_6$ films and FMI states observed in underdoped manganites. In manganites, i.e., $La_{1-x}Sr_xMnO_3$, while the optimal doping ($x = 0.3$) stabilize a FMM state, a peculiar FMI state emerges in a lightly doped region ($0.1 < x < 0.17$).[42] This metal–insulator transition with robust ferromagnetism by changing the valence of Mn is phenomenologically similar to our observation in the $Sr_2Fe_{1+x}Re_{1-x}O_6$ system. Therefore, these phase similarities between $La_{1-x}Sr_xMnO_3$ and $Sr_2Fe_{1+x}Re_{1-x}O_6$ imply that intriguing physics intensively studied in manganites may also exist in the latter system, such as the phase separation, coexistence of FMM and antiferromagnetic insulating phases, and colossal magnetoresistance.[42] Further studies on $Sr_2Fe_{1+x}Re_{1-x}O_6$, therefore, are

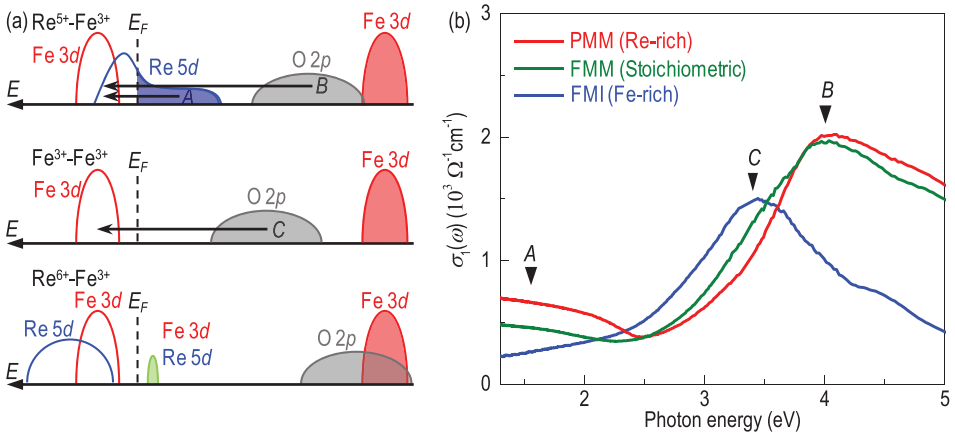

Figure 4. Electronic structures and optical conductivity of $Sr_2Fe_{1+x}Re_{1-x}O_6$ films. a) Local DOS of three types of bonding in an Fe-rich film based on reported DFT calculations.[17,38,39] The expected optical transitions in Fe^{3+}—Re^{5+} and Fe^{3+}—Fe^{3+} bonding were denoted as *A*, *B*, and *C*. b) $\sigma_1(\omega)$ of PMM, FMM, and FMI films: The three expected optical transitions are observed in the spectra of FMM and FMI films.

highly encouraged. One noticeable difference between these two cases, however, is the robustness of T_c. T_c in underdoped manganites has strong doping dependence with depletion of charge carriers, whereas the stoichiometry effect on T_c in the double-perovskite system is minuscule. This difference might be attributed to hybridization-induced ferromagnetic interactions, which is known to be irrelevant to free carriers in double perovskites, thereby, providing an excellent playground to search for high-T_c FMIs.

In summary, we discovered a new room-*T* FMI by deliberately controlling the ratio of two B-site cations in the double perovskite $Sr_2Fe_{1+x}Re_{1-x}O_6$. A single growth parameter P_{O_2} was used to control the cation ordering and ratio. Particularly in the Fe-rich/ordered growth regime, we found an intriguing FMI state which was attributed to excess Fe^{3+} and emergent Re^{6+} ions. Our results provide a new promising route to developing oxide FMIs, useful for applications in spin filter, magnetic proximity, and quantum anomalous Hall effects. This new FMI may also enable the development of energy efficient quantum electronic and spintronic devices.

Experimental Section

Synthesis of $Sr_2Fe_{1+x}Re_{1-x}O_6$ Films: Pulsed laser deposition was used to grow high-quality $Sr_2Fe_{1+x}Re_{1-x}O_6$ films in a wide range of growth parameters, such as temperature (T = 650–775 °C), oxygen partial pressure (P_{O_2} = 0.1–100 mTorr), laser fluence (1–2 J cm^{-2}), and laser repetition rate (1–10 Hz). Among the growth parameters, oxygen partial pressure turned out to be the most critical parameter for cation ordering and stoichiometry control. Therefore, the samples presented here were grown at fixed conditions after extensive optimization processes—*T* (775 °C), laser fluence (1.5 J cm^{-2}), and frequency (5 Hz—except the P_{O_2}. All the films used in this work were 30–40 nm in thickness.

Basic Characterization: High-resolution four circle XRD, superconducting quantum interference device, and physical property measurement system were used to check the crystallographic, magnetic, and transport properties of thin films, respectively.

Scanning Transmission Electron Microscopy: Cross-sectional specimens for STEM imaging were prepared using ion milling after mechanical thinning and precision polishing. HAADF imaging was carried out in a Nion UltraSTEM100 operated at 100 keV. The microscope was equipped with a cold field-emission gun and an aberration corrector for sub-angstrom resolution. An inner detector angle of 78 mrad was used for imaging. The convergence semi-angle for the electron probe was set to 30 mrad.

Rutherford Back-Scattering Spectrometry: RBS technique was used to determine the Re/Fe ratio in the films. A parallel 2.0 MeV He beam was employed in these measurements with a detector located underneath the He beam at a backscattering angle of 168° and solid angle of 2.3×10^{-3} sr to have a combining advantage of optimized mass resolution and depth resolution.[43]

X-Ray Absorption Spectroscopy: Fe *L*-edge spectra were obtained at the beamline 4-ID-C of Advanced Photon Source at 50 K with total electron and FY modes. The Re *L*-edge spectra were taken at the beamline 4-ID-D of Advanced Photon Source with an energy dispersive detector by collecting the Re L_α and Re L_β fluorescence lines, respectively, for the L_3 and L_2 edges.

Spectroscopic Ellipsometry: By using an M-2000 ellipsometer (J. A. Woollam Co.), two ellipsometric parameters, ψ and Δ, for a thin film and a bare $SrTiO_3$ substrate were obtained at room temperature. A two-layer model composed of the substrate and the film was constructed to determine the optical constant of the film.

Acknowledgements

This work was supported by the U.S. Department of Energy (DOE), Office of Science, Basic Energy Sciences, Materials Sciences and Engineering Division. This research used resources of the Center for Nanophase Materials Sciences (spectroscopic ellipsometry and STEM), which is a DOE Office of Science User Facility. Use of the Advanced Photon Source, which is also a DOE Office of Science User Facility, was supported by the US DOE, Office of Science, under Contract No. DE-AC02-06CH11357. L.N. was supported for the RBS work by the University of Tennessee Governor's Chair program.

Conflict of Interest

The authors declare no conflict of interest.

Keywords

epitaxy, ferromagnetic insulators, oxide perovskites, spectroscopy, Sr_2FeReO_6

Received: August 17, 2018
Revised: October 23, 2018
Published online: November 29, 2018

[1] D. P. DiVincenzo, *J. Appl. Phys.* **1999**, *85*, 4785.
[2] H. Haugen, D. Huertas-Hernando, A. Brataas, *Phys. Rev. B* **2008**, *77*, 115406.
[3] H. Yang, A. Hallal, D. Terrade, X. Waintal, S. Roche, M. Chshiev, *Phys. Rev. Lett.* **2013**, *110*, 046603.
[4] S. Sakai, S. V. Erohin, Z. I. Popov, S. Haku, T. Watanabe, Y. Yamada, S. Entani, S. Li, P. V. Avramov, H. Naramoto, K. Ando, P. B. Sorokin, Y. Yamauchi, *Adv. Funct. Mater.* **2018**, *28*, 1800462.
[5] I. Vobornik, U. Manju, J. Fujii, F. Borgatti, P. Torelli, D. Krizmancic, Y. S. Hor, R. J. Cava, G. Panaccione, *Nano Lett.* **2011**, *11*, 4079.
[6] C. Tang, C.-Z. Chang, G. Zhao, Y. Liu, Z. Jiang, C.-X. Liu, M. R. McCartney, D. J. Smith, T. Chen, J. S. Moodera, *Sci. Adv.* **2017**, *3*, e1700307.
[7] M. A. Ruderman, C. Kittel, *Phys. Rev.* **1954**, *96*, 99.
[8] T. Kasuya, *Prog. Theor. Phys.* **1956**, *16*, 45.
[9] K. Yosida, *Phys. Rev.* **1957**, *106*, 893.
[10] D. Meng, H. Guo, Z. Cui, C. Ma, J. Zhao, J. Lu, H. Xu, Z. Wang, X. Hu, Z. Fu, *Proc. Natl. Acad. Sci. U.S.A.* **2018**, *115*, 2873.
[11] K. I. Kobayashi, T. Kimura, H. Sawada, K. Terakura, Y. Tokura, *Nature* **1998**, *395*, 677.
[12] T. Kim, M. Uehara, S. Cheong, S. Lee, *Appl. Phys. Lett.* **1999**, *74*, 1737.
[13] K.-I. Kobayashi, T. Kimura, Y. Tomioka, H. Sawada, K. Terakura, Y. Tokura, *Phys. Rev. B* **1999**, *59*, 11159.
[14] Y. Tomioka, T. Okuda, Y. Okimoto, R. Kumai, K.-I. Kobayashi, Y. Tokura, *Phys. Rev. B* **2000**, *61*, 422.
[15] H. Kato, T. Okuda, Y. Okimoto, Y. Tomioka, Y. Takenoya, A. Ohkubo, M. Kawasaki, Y. Tokura, *Appl. Phys. Lett.* **2002**, *81*, 328.
[16] D. Serrate, J. De Teresa, M. Ibarra, *J. Phys.: Condens. Matter* **2007**, *19*, 023201.
[17] Z. Fang, K. Terakura, J. Kanamori, *Phys. Rev. B* **2001**, *63*, 180407.
[18] D. Sarma, P. Mahadevan, T. Saha-Dasgupta, S. Ray, A. Kumar, *Phys. Rev. Lett.* **2000**, *85*, 2549.
[19] H. Kato, T. Okuda, Y. Okimoto, Y. Tomioka, K. Oikawa, T. Kamiyama, Y. Tokura, *Phys. Rev. B* **2004**, *69*, 184412.
[20] A. Hauser, J. Soliz, M. Dixit, R. Williams, M. Susner, B. Peters, L. Mier, T. Gustafson, M. Sumption, H. Fraser, *Phys. Rev. B* **2012**, *85*, 161201.
[21] S. Chakraverty, A. Ohtomo, M. Kawasaki, *Appl. Phys. Lett.* **2010**, *97*, 243107.
[22] T. Manako, M. Izumi, Y. Konishi, K.-I. Kobayashi, M. Kawasaki, Y. Tokura, *Appl. Phys. Lett.* **1999**, *74*, 2215.
[23] W. Westerburg, D. Reisinger, G. Jakob, *Phys. Rev. B* **2000**, *62*, R767.
[24] D. Sánchez, M. García-Hernández, N. Auth, G. Jakob, *J. Appl. Phys.* **2004**, *96*, 2736.
[25] A. J. Hauser, R. E. Williams, R. A. Ricciardo, A. Genc, M. Dixit, J. M. Lucy, P. M. Woodward, H. L. Fraser, F. Yang, *Phys. Rev. B* **2011**, *83*, 014407.
[26] E. Cazzanelli, M. Castriota, S. Marino, N. Scaramuzza, J. Purans, A. Kuzmin, R. Kalendarev, G. Mariotto, G. Das, *J. Appl. Phys.* **2009**, *105*, 114904.
[27] B. Yildiz, *MRS Bull.* **2014**, *39*, 147.
[28] J. R. Petrie, C. Mitra, H. Jeen, W. S. Choi, T. L. Meyer, F. A. Reboredo, J. W. Freeland, G. Eres, H. N. Lee, *Adv. Funct. Mater.* **2016**, *26*, 1564.
[29] T. L. Meyer, R. Jacobs, D. Lee, L. Jiang, J. W. Freeland, C. Sohn, T. Egami, D. Morgan, H. N. Lee, *Nat. Commun.* **2018**, *9*, 92.
[30] T.-W. Lim, S.-D. Kim, K.-D. Sung, Y.-M. Rhyim, H. Jeen, J. Yun, K.-H. Kim, K.-M. Song, S. Lee, S.-Y. Chung, *Sci. Rep.* **2016**, *6*, 19746.
[31] H. Kato, T. Okuda, Y. Okimoto, Y. Tomioka, K. Oikawa, T. Kamiyama, Y. Tokura, *Phys. Rev. B* **2002**, *65*, 144404.
[32] J. De Teresa, D. Serrate, J. Blasco, M. Ibarra, L. Morellon, *Phys. Rev. B* **2004**, *69*, 144401.
[33] J. De Teresa, J. Michalik, J. Blasco, P. Algarabel, M. Ibarra, C. Kapusta, U. Zeitler, *Appl. Phys. Lett.* **2007**, *90*, 252514.
[34] M. Abe, T. Nakagawa, S. Nomura, *J. Phys. Soc. Jpn.* **1973**, *35*, 1360.
[35] J. Everett, E. Céspedes, L. Shelford, C. Exley, J. Collingwood, J. Dobson, G. van der Laan, C. Jenkins, E. Arenholz, N. Telling, *J. R. Soc., Interface* **2014**, *11*, 20140165.
[36] M. Abbate, F. M. de Groot, J. Fuggle, A. Fujimori, O. Strebel, F. Lopez, M. Domke, G. Kaindl, G. Sawatzky, M. Takano, *Phys. Rev. B* **1992**, *46*, 4511.
[37] J. Herrero-Martín, G. Subías, J. Blasco, J. García, M. Sánchez, *J. Phys.: Condens. Matter* **2005**, *17*, 4963.
[38] H. Wu, *Phys. Rev. B* **2001**, *64*, 125126.
[39] M. D. Scafetta, A. M. Cordi, J. M. Rondinelli, S. J. May, *J. Phys.: Condens. Matter* **2014**, *26*, 505502.
[40] B. Jeon, C. H. Kim, S. Moon, W. S. Choi, H. Jeong, Y. Lee, J. Yu, C. Won, J. Jung, N. Hur, *J. Phys.: Condens. Matter* **2010**, *22*, 345602.
[41] T.-h. Arima, Y. Tokura, *J. Phys. Soc. Jpn.* **1995**, *64*, 2488.
[42] Y. Tokura, *Rep. Prog. Phys.* **2006**, *69*, 797.
[43] Y. Zhang, M. L. Crespillo, H. Xue, K. Jin, C.-H. Chen, C. L. Fontana, J. Graham, W. J. Weber, *Nucl. Instrum. Methods Phys. Res., Sect. B* **2014**, *338*, 19.